Chemical Papers
https://doi.org/10.1007/s11696-025-04507-5

ORIGINAL PAPER

Interfacial electrochemistry and diffusion dynamics in Si@Nb_2O_5 anodes: a multiphysics approach

Suleiman Ibrahim Mohammad[1,2] · Asokan Vasudevan[3,4] · Hüseyin Kurt[5] · B. R. Sampangi Rama Reddy[6] · Zahraa AlKhafaje[7] · S. Gayathri[8,9] · Aneesh Wunnava[10] · Renu Sharma[11] · Anita Gehlot[12] · Amir Arsalanirad[13]

Received: 14 September 2025 / Accepted: 10 November 2025

Abstract
The development of high-performance anode materials is essential for advancing lithium-ion battery (LIB) technology. Silicon (Si) is a promising candidate due to its high theoretical capacity and abundance; however, its practical application is hindered by severe volume expansion and unstable solid electrolyte interphase (SEI) formation during lithiation. This study investigates the chemical and electrochemical mechanisms by which a niobium pentoxide (Nb_2O_5) nanolayer enhances the performance of Si-based anodes through finite element modeling in COMSOL Multiphysics. The Nb_2O_5 coating, characterized by high ionic diffusivity and electrical conductivity resulting from oxygen vacancies and lattice distortions, acts as a chemically robust interface that mitigates SEI degradation, reduces interfacial polarization, and stabilizes charge transfer dynamics. A parametric analysis of coating thickness (2.5–15 nm) reveals that a 10 nm Nb_2O_5 layer offers optimal performance by minimizing lithium-ion concentration gradients (an 18% reduction), lowering SEI potential drop (a 44% reduction), and improving current density uniformity during the first charge–discharge cycle. These improvements stem from the interplay between defect-driven transport mechanisms and interface stabilization. The findings provide a comprehensive chemical framework for designing next-generation anode materials with enhanced stability, reversibility, and cycle life, with significant implications for high-efficiency energy storage systems.

Keywords Solid electrolyte interphase (SEI) · Defect chemistry · Lithium-Ion diffusion · Surface coating chemistry · Interfacial electrochemistry

✉ Amir Arsalanirad
amirarsalaniradacademic@gmail.com

[1] Electronic Marketing and Social Media, Economic and Administrative Sciences, Zarqa University, Zarqa, Jordan

[2] INTI International University, 71800 Nilai, Negeri Sembilan, Malaysia

[3] Faculty of Business and Communications, INTI International University, 71800 Nilai, Negeri Sembilan, Malaysia

[4] Shinawatra University, 99 Moo 10, Bangtoey, Samkhok 12160, Pathum Thani, Thailand

[5] Department of Electrical and Electronics Engineering, Faculty of Engineering, Istanbul Aydın University, Istanbul, Turkey

[6] Department of Physics & Electronics, School of Sciences, JAIN (Deemed to Be University), Bangalore, Karnataka, India

[7] Department of Medical Analysis, Medical Laboratory Technique College, The Islamic University, Najaf, Iraq

[8] Department of Chemistry, Sathyabama Institute of Science and Technology, Chennai, Tamil Nadu, India

[9] Sharda School of Engineering and Science, Sharda University, Greater Noida, India

[10] Department of Electronics & Communication Engineering, Siksha 'O' Anusandhan (Deemed to Be University), Bhubaneswar, Odisha 751030, India

[11] Department of Chemistry, University Institute of Sciences, Chandigarh University, Mohali, Punjab, India

[12] Uttaranchal Institute of Technology, Uttaranchal University, Dehradun, Uttarakhand 248007, India

[13] Young Researchers and Elite Club, Tehran University, Tehran, Iran

Published online: 28 November 2025

Introduction

Lithium-ion batteries (LIBs) are pivotal to modern energy storage, driven by their high energy density and versatility across applications such as portable electronics, electric vehicles, and grid-scale systems (Sharma et al. 2025; Singh et al. 2024). The quest for advanced anode materials to enhance LIB performance has spotlighted silicon (Si) due to its exceptional theoretical specific capacity (~3579 mAh/g for $Li_{15}Si_4$), low lithiation potential (~0.1 V vs. Li/Li^+), and elemental abundance (Feng et al. 2018). However, the chemical complexity of Si anodes poses significant challenges to their practical implementation. During lithiation, Si undergoes a dramatic volume expansion of up to 300%, triggering mechanical stress that disrupts the anode's structural integrity and promotes continuous formation of the solid electrolyte interphase (SEI) layer via electrolyte decomposition (Khan et al. 2024; Sun et al. 2022). The SEI, primarily composed of lithium salts (e.g., Li_2CO_2, LiF) and organic compounds, exhibits poor ionic and electronic conductivity (typically 10^{-7} S/m), creating a resistive barrier that impedes Li^+ diffusion, increases charge transfer resistance, and accelerates capacity fade (Adenusi et al. 2023; Xu 2024). These issues are deeply rooted in the chemical interactions at the anode-electrolyte interface, where uncontrolled SEI growth and irreversible side reactions destabilize electrochemical performance (Chen et al. 2022; Di et al. 2021). The defect chemistry of the anode surface, coupled with the SEI's heterogeneous composition, further exacerbates polarization and hinders efficient Li^+ intercalation, necessitating innovative chemical strategies to stabilize the interface and enhance electrochemical reversibility (Li et al. 2023; Wang et al. 2024).

Surface modification through protective coatings has emerged as a promising approach to address these chemical challenges, with metal oxides like niobium pentoxide ($Nb_2O_5Nb_2O_5$) showing particular promise due to their unique chemical properties (Liu et al. 2024). Nb_2O_5 exhibits high ionic diffusivity (10^{-14} to 10^{-13} cm^2/s) and electrical conductivity (10^{-6} S/m), driven by a defect-rich crystalline structure characterized by oxygen vacancies and lattice distortions that facilitate rapid Li^+ and electron transport (Kim et al. 2025; Lim 2025). These defects lower the activation energy for Li^+ diffusion and enhance charge delocalization, reducing interfacial polarization and stabilizing the SEI against continuous growth (Ma & Xu 2023). Recent studies have demonstrated that Nb_2O_5-coated Si anodes exhibit improved cycle stability and coulombic efficiency, attributed to the coating's ability to form a chemically robust interface that mitigates electrolyte decomposition and buffers volume expansion-induced stress (Ma et al. 2023). The chemical composition and defect structure of Nb_2O_5 enable it to act as a passivating layer, reducing parasitic reactions while maintaining efficient ion transport pathways (Xu et al. 2021).

Recent advances in Si-based anodes highlight innovative surface modifications and structural designs to mitigate volume expansion and enhance conductivity. Liu et al. (2025) introduced inorganic SiO_x with higher valence in core–shell Si@SiO_x/C composites, achieving 1163 mAh g^{-1} after 400 cycles at 1 A g^{-1} via improved structural stability. Han et al. (2024) developed honeycomb porous Si using a safe Stöber-magnesium reduction route, delivering 824.1 mAh g^{-1} at 0.5 A g^{-1} with reduced agglomeration. Qin et al. (2020) synthesized single-crystalline T-Nb_2O_5 nanorods from Nb_2CT_x MXene, enabling fast Li^+ intercalation and 95% retention over 4000 cycles in Li-ion capacitors. These works underscore the critical role of defect-rich, high-valence oxide interfaces—directly supporting the superior interfacial stabilization and transport efficiency of the 10 nm Nb_2O_5 coating in this study.

However, the efficacy of Nb_2O_5 coatings is highly sensitive to their thickness, as excessive thickness may introduce resistive losses due to defect clustering or extended diffusion pathways, while insufficient thickness fails to provide adequate chemical protection (Liu et al. 2024). Optimizing these chemical properties requires a detailed understanding of the interplay between coating thickness, defect chemistry, and interfacial reactivity, particularly in the context of SEI stabilization and Li^+ transport dynamics.

Computational modeling has become a critical tool for elucidating the chemical mechanisms governing LIB anode performance, offering insights into the molecular and atomic interactions that dictate electrochemical behavior (Alkhedher et al. 2024; Nourizadeh et al. 2025). Finite element methods, implemented in platforms like COMSOL Multiphysics, solve coupled partial differential equations to simulate Li^+ diffusion, charge transfer kinetics, and SEI evolution, capturing the impact of defect chemistry on ion transport and interfacial stability (Jiao et al. 2023; Lee et al. 2022). Recent studies have employed such models to investigate how coating materials modulate concentration gradients, electric potential distributions, and reaction rates, providing a predictive framework for optimizing anode architectures (Lopata et al. 2023). These computational approaches are particularly valuable for studying Si-based anodes, where the interplay between chemical composition, defect structures, and electrochemical performance is complex and multifaceted (Song et al. 2024). By integrating experimental data with simulations, researchers can correlate microscopic chemical interactions (such as oxygen vacancy-mediated ion diffusion) with macroscopic electrochemical properties, enabling the design of chemically stable and efficient anode materials (Benayad et al. 2022).

Despite these advancements, the chemical optimization of Nb_2O_5 coatings for Si anodes remains underexplored, particularly in terms of tailoring thickness to balance ionic and electronic transport while minimizing resistive losses. This study addresses these gaps through numerical simulations using COMSOL Multiphysics, solving coupled equations for Li^+ transport, electrochemical reaction kinetics, charge conservation, SEI growth, and mechanical/thermal effects. By systematically investigating the effect of Nb_2O_5 coating thickness (2.5–15 nm) on the electrochemical performance of Si@Nb_2O_5 core–shell anodes during the first charge–discharge cycle, this work aims to elucidate the chemical mechanisms (such as defect-driven Li^+ diffusion, interfacial stabilization, and SEI chemistry) that govern anode performance. The study seeks to provide a robust chemical framework for designing high-performance LIB anode materials, with significant implications for energy storage applications requiring enhanced cycle life and electrochemical efficiency.

Materials and methods

Governing equations

The numerical investigation of the Si@Nb_2O_5 core–shell anode and its impact on the stability of the solid electrolyte interphase layer was conducted by solving a coupled set of partial differential equations (PDEs). These equations govern lithium-ion (Li^+) transport, electrochemical reaction kinetics, charge conservation, mechanical stress effects, SEI growth and dissolution, and thermal effects. The equations, implemented in COMSOL Multiphysics, describe the electrochemical, mechanical, and thermal behavior of the system, with parameters derived from experimental data (Wang et al. 2016).

Lithium-ion transport

Lithium-ion (Li^+) diffusion in the Nb_2O_5 nanolayer and SEI is governed by a modified Fick's second law, incorporating concentration-dependent diffusion (Wolfrum et al. 1988):

$$\frac{\partial c}{\partial t} = \nabla.\left(D\left(c\right)\nabla c\right) \tag{1}$$

where c is the Li^+ concentration (mol/m^3), t is time (s), and D(c) is the concentration-dependent diffusion coefficient (cm^2/s), defined as:

$$D\left(c\right) = D_0\left(1 - \frac{c}{c_{\max}}\right) \tag{2}$$

Here, D_0 is the baseline diffusion coefficient and c_{max} is the maximum Li^+ concentration. Equation (1) governs diffusive Li^+ transport, with Eq. 2 accounting for reduced diffusivity at high concentrations due to crowding effects in the SEI.

Electrochemical reaction kinetics

The electrochemical reaction at the anode-electrolyte interface (lithium intercalation into silicon) is described by the Butler-Volmer equation, modified to include concentration overpotential (Dickinson & Wain 2020):

$$i = i_0\left[\exp\left(\frac{nF\left(\eta - \eta_c\right)\left(1-\alpha\right)}{RT}\right) - \exp\left(\frac{-\alpha nF\left(\eta - \eta_c\right)}{RT}\right)\right] \tag{3}$$

where i is the current density (A/m^2), i_0 is the exchange current density, α is the charge transfer coefficient, n is the number of electrons transferred, F is Faraday's constant (96,485 C/mol), η is the activation overpotential (V), η_c is the concentration overpotential (V), R is the gas constant (8.314 J/mol.K), and T is the temperature. The concentration overpotential is defined as:

$$\eta_c = \frac{RT}{nF}\ln\left(\frac{c_{surface}}{c_{bulk}}\right) \tag{4}$$

where $c_{surface}$ and c_{bulk} are the Li^+ concentrations at the electrode surface and in the bulk electrolyte (1000 mol/m^3), respectively. The charge transfer resistance for the Si@Nb_2O_5 composite was incorporated via i_0.

Charge conservation

The electric potential distribution in the conductive domains (silicon core, Nb_2O_5, and SEI) is governed by charge conservation (Rueckner 2007):

$$\nabla.\left(\sigma\nabla\phi\right) = 0 \tag{5}$$

where φ is the electric potential (V), and σ is the electrical conductivity. The ionic current density in the SEI is expressed as:

$$i = -\sigma\nabla\phi \tag{6}$$

Coupled ion and electron transport in the electrolyte and SEI is described by the Nernst-Planck equation (Maex 2015):

$$J = -D\nabla c - \frac{zFDc}{RT}\nabla\phi \tag{7}$$

where J is the total Li^+ flux (mol/m^2.s), z is the ion charge, and the second term represents migration due to the electric field.

Advanced SEI growth and dissolution

The evolution of the SEI layer, including growth from irreversible electrolyte decomposition and partial dissolution, is modeled by a dynamic equation for SEI thickness (δ_{SEI}) (Jha & Krishnamurthy 2022):

$$\frac{\partial \delta_{SEI}}{\partial t} = k_{SEI} i_{side} - k_{diss} \delta_{SEI} \tag{8}$$

where δ_{SEI} is the SEI thickness (m), k_{SEI} is the SEI formation rate constant, i_{side} is the side reaction current density, and k_{diss} is the SEI dissolution rate constant. The ionic conductivity of the SEI (σ_{SEI}) depends on thickness:

$$\sigma_{SEI} = \sigma_0 \exp\left(-\frac{\delta_{SEI}}{\delta_0}\right) \tag{9}$$

where σ_0 is the baseline SEI conductivity and δ_0 is a characteristic thickness. Equation (8) captures SEI growth during cycling, while Eq. (9) reflects the impact of thickness on ion transport.

Mechanical stress effects

Volume expansion in the silicon core during lithiation induces mechanical stress, governed by the linear elastic stress equation (Dixit & Dixit 2008):

$$\nabla . \sigma_{mech} = 0 \tag{10}$$

where σ_{mech} is the stress tensor (Pa). The stress is related to the strain (ε) via Hooke's law (Dell'Isola et al. 2009):

$$\sigma_{mech} = C : \varepsilon \tag{11}$$

where C is the stiffness tensor for silicon, and ε includes contributions from lithiation-induced volume expansion. The stress affects the diffusion coefficient via:

$$D\left(c, \sigma_{mech}\right) = D_0 \exp\left(-\frac{\sigma_{mech} V_m}{RT}\right) \tag{12}$$

where V_m is the molar volume of silicon. Equation 12 couples mechanical stress to Li^+ diffusion.

Thermal effects

Thermal effects from electrochemical reactions and joule heating are governed by the heat transfer equation (Yuan et al. 2024):

$$\rho C_p \frac{\partial T}{\partial t} = \nabla . (k \nabla T) + Q \tag{13}$$

where ρ is the material density, C_p is the specific heat capacity, k is the thermal conductivity, and Q is the heat source (W/m^3), comprising joule heating and reaction heat:

$$Q = \sigma \left|\nabla \phi\right|^2 + i\eta \tag{14}$$

where σ $|\nabla \varphi|^2$ represents joule heating, and i η represents heat from electrochemical reactions (i from Eq. (3), η from Eq. (4)). The temperature couples to Eqs. (3), (7), and (12) via the temperature-dependent terms. The initial temperature is set to 298 K, with boundary conditions assuming convective heat transfer to the environment (h = 7 W/m^2.K (Hosseinzadeh et al. 2018; Lai et al. 2015; Tourani et al. 2014)).

Numerical implementation

The numerical investigation was conducted using COMSOL Multiphysics to solve the governing equations Eqs. (1)–(14), coupling the transport of diluted species, secondary current distribution, solid mechanics, and heat transfer in solids modules. A 2D axisymmetric geometry was constructed to represent the Si@Nb_2O_5 core–shell anode, enabling efficient modeling of radial ion, charge, stress, and heat transport. The geometry consisted of a silicon core, Nb_2O_5 coating, and SEI layer interfacing with the electrolyte. The total computational domain spanned 0–60 nm, with the Nb_2O_5 layer occupying 0–10 nm, the SEI layer 10–50 nm, and the silicon anode surface at 50–60 nm. These dimensions were derived from transmission electron microscopy (TEM) data reported by Wang et al. (2016). Material properties were assigned based on experimental data from (Wang et al. 2016), supplemented with literature values where necessary, as detailed in Table 1.

Boundary conditions were defined to simulate electrochemical, mechanical, and thermal behavior:

- At the anode surface (Si-Nb_2O_5 interface), lithium intercalation was modeled using Eq. (3) within a potential window of 0.01–1.5 V vs. Li/Li^+, consistent with experimental conditions. Mechanical boundary conditions imposed fixed constraints to account for stress from volume expansion.

Table 1 Material properties of $Si@Nb_2O_5$ core–shell anode components and electrolyte

Component	Property	Value	Unit	Note
Silicon core	Density	2.33	g/cm^3	Exp. Wang et al. (2016)
	Electrical conductivity	10^{-3}	S/m	Exp. Wang et al. (2016)
	Young's modulus	150	GPa	Lit. Dixit & Dixit (2008)
	Thermal conductivity	150	W/m.K	Exp. Wang et al. (2016)
	Specific heat capacity	700	J/kg·K	Exp. Wang et al. (2016)
Nb_2O_5 nanolayer	Ionic diffusivity	10^{-14}	cm^2/s	EIS Wang et al. (2016)
	Electrical conductivity	10^{-6}	S/m	Lit. Kim et al. (2025)
	Thermal conductivity	0.5	W/m.K	Lit. Wang et al. (2016)
	Specific heat capacity	500	J/kg.K	Lit. Wang et al. (2016)
SEI layer	Ionic diffusivity	10^{-15}	cm^2/s	EIS Wang et al. (2016)
	Ionic conductivity	10^{-7}	S/m	Exp. Wang et al. (2016)
	Thermal conductivity	0.1	W/m·K	Lit. Wang et al. (2016)
	Specific heat capacity	1000	J/kg.K	Lit. Wang et al. (2016)
Electrolyte	Li^+ concentration	1	mol/L	Mod. (infinite reservoir)

- At the Nb_2O_5-SEI interface, limited ion and electron transfer was modeled using Eq. (7), with stress continuity enforced.
- At the electrolyte-SEI interface, a constant Li^+ concentration of 1 mol/L and convective heat transfer (heat transfer coefficient = 10 $W/m^2 \cdot K$) were applied.
- Along the symmetry axis, zero-flux conditions were imposed to maintain axisymmetric behavior.

Model validation

The numerical model, implemented in COMSOL Multiphysics to solve Eqs. (1)–(14), was validated against experimental data reported by Wang et al. (2016). Specifically, the simulated current density–voltage profile for the first charge–discharge cycle of the $Si@Nb_2O_5$ core–shell anode was compared with experimental results presented in (Wang et al. 2016). The experimental data from (Wang et al. 2016) was used to validate the numerical simulations in this study, ensuring the accuracy of the modeled lithium-ion transport and electrochemical reaction kinetics.

To quantify the agreement between the simulation and experimental results, the root mean square error (RMSE) was calculated for the current density–voltage profile of the first cycle. The RMSE was determined to be 0.7, indicating high accuracy and close alignment between the simulated and experimental data. This low error value confirms the robustness of the numerical model in capturing the electrochemical behavior of the $Si@Nb_2O_5$ nanocomposite, including lithium-ion transport, reaction kinetics, and SEI stability. These results validate the reliability of the governing equations and numerical implementation in predicting the electrochemical performance of the $Si@Nb_2O_5$ core–shell anode.

Simulation of current density–voltage profiles

The current density–voltage (i–V) profiles shown in Fig. 1 were obtained by imposing a galvanostatic charge–discharge protocol at a specific current density of 0.1 A/g (corresponding to ~ 0.036 mA/cm^2 based on the active material mass loading derived from Ref. Wang et al. (2016). The simulation was run in the "Time Dependent" study with a voltage-controlled boundary condition at the electrolyte domain (fixed Li/Li^+ reference at 0 V) and a current density boundary condition at the silicon core Eq. ((3) implemented via a "Flux" boundary node). The voltage was linearly swept from 1.5 V to 0.01 V (lithiation) and back to 1.5 V (delithiation) over a total cycle time of ~ 2 × 3600 s (adjusted to match the experimental C-rate). At each time step, the local current density at the anode surface (r = 50 nm) was extracted using a surface integration probe defined over the $Si–Nb_2O_5$ interface. The resulting time-dependent current density was plotted against the cell voltage (computed as the potential difference between the anode surface and the Li reference) to generate Fig. 1. A relative tolerance of 10^{-6} and an automatic time-stepping (maximum step 10 s) ensured convergence. The simulated profile was directly compared with the experimental data from Wang et al. (2016), yielding an RMSE of 0.7, confirming the fidelity of the multiphysics coupling.

Results

Numerical simulations of the $Si@Nb_2O_5$ core–shell anode were conducted using COMSOL Multiphysics to solve Eqs. (1)–(14) for the first charge–discharge cycle at a current density of 0.1 A/g. The results, presented in four subsections (ion concentration profiles, electric potential distribution, reaction rate and current density, and a parametric study) analyze the electrochemical performance for configurations with Nb_2O_5 coatings (2.5, 5, 7.5, 10, 12.5, 15 nm) and without Nb_2O_5. The data, detailed in Figs. 2–4, were validated against experimental results from Wang et al.

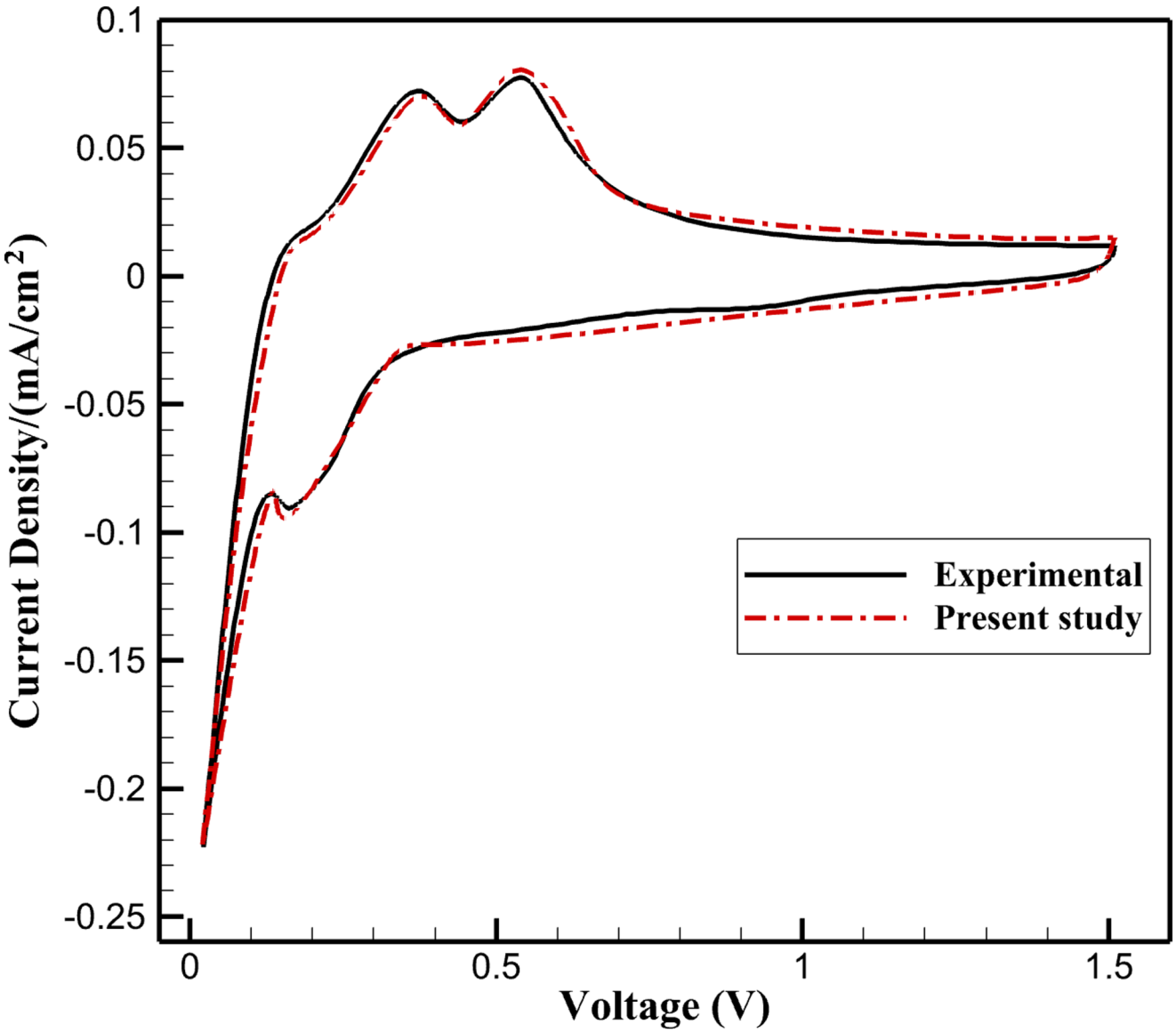

Fig. 1 Comparison of simulated (solid line) and experimental (symbols) current density–voltage profiles for the first galvanostatic charge–discharge cycle of the Si@Nb_2O_5 nanocomposite anode at 0.1 A/g (voltage sweep: 0.01–1.5 V vs. Li/Li^+). Simulation performed via surface integration of local current density at the Si–Nb_2O_5 interface

(2016), achieving a root mean square error (RMSE) of 0.7 for the current density–voltage profile.

Ion concentration profiles

The lithium-ion concentration profiles across the solid electrolyte interphase layer of the Si@Nb_2O_5 core–shell anode were investigated during the first charge–discharge cycle at a current density of 0.1 A/g, using a modified Fick's second law coupled with the Nernst-Planck equation to model ion transport dynamics. Figure 2 presents the concentration profiles for configurations with Nb_2O_5 coatings (2.5, 5, 7.5, 10, 12.5, 15 nm) and without Nb_2O_5, elucidating the chemical role of the Nb_2O_5 nanolayer in enhancing Li^+ diffusion and mitigating interfacial polarization. The Nb_2O_5 coating, with an ionic diffusivity of 10^{-14} to 10^{-13} cm^2/s, facilitates efficient Li^+ transport, reducing concentration gradients and stabilizing the electrochemical interface.

The 10 nm Nb_2O_5 coating exhibited the most uniform concentration profile, with Li^+ concentrations decreasing smoothly from 940 mol/m^3 at the Nb_2O_5-SEI interface to 790 mol/m^3 at the SEI-electrolyte interface. This profile corresponds to an 18% reduction in polarization compared to the uncoated configuration (980 to 700 mol/m^3), attributed to the Nb_2O_5 layer's ability to enhance Li^+ diffusion and minimize ion accumulation at the anode-SEI interface. The

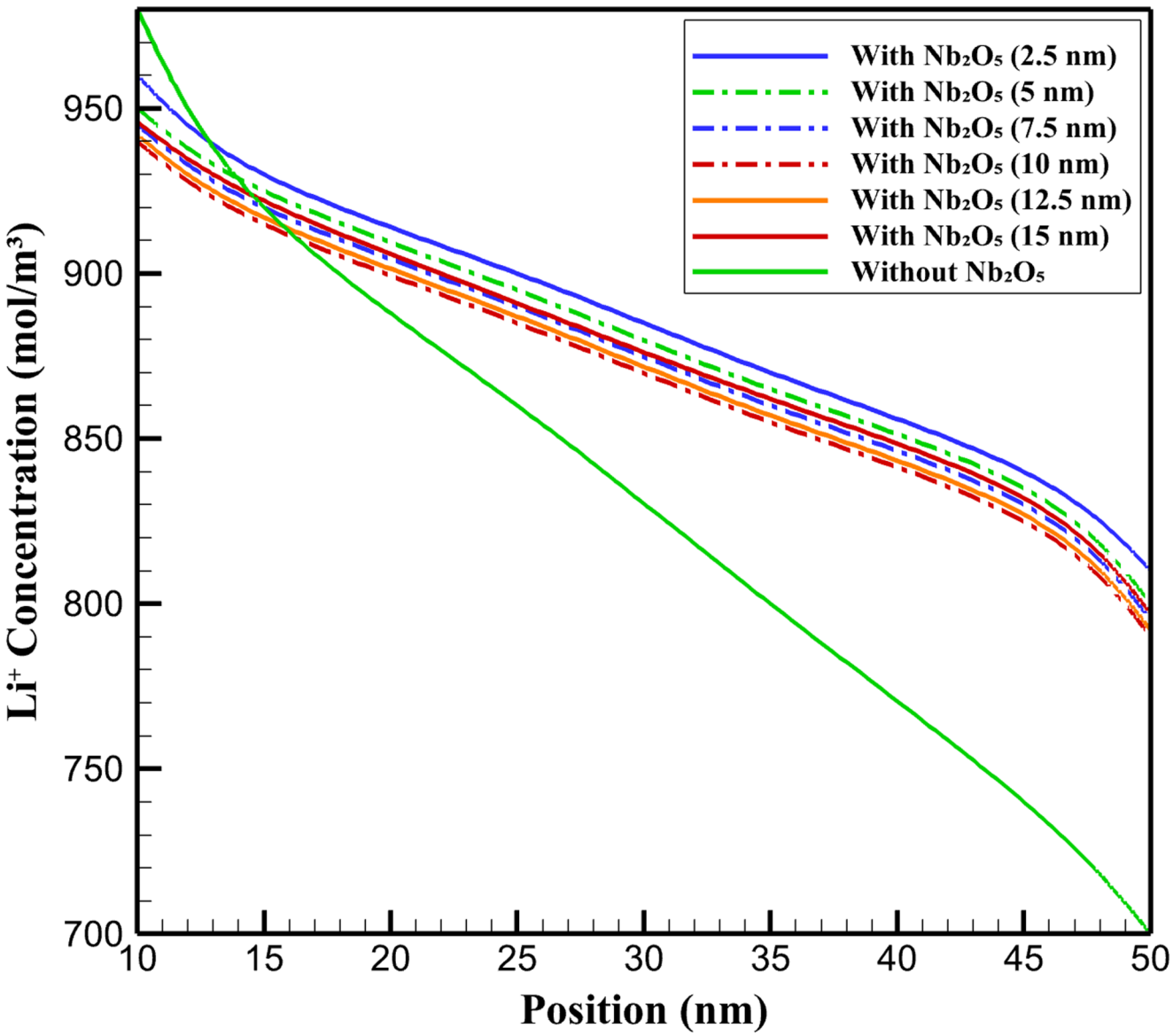

Fig. 2 Li^+ concentration profiles across the SEI layer during the first charge–discharge cycle at 0.1 A/g. Key values at Nb_2O_5–SEI interface (r = 10 nm): uncoated: 980 mol/m^3; 2.5 nm: 960 mol/m^3; 5 nm: 950 mol/m^3; 7.5 nm: 945 mol/m^3; 10 nm: 940 mol/m^3 (optimal); 12.5 nm: 942 mol/m^3; 15 nm: 945 mol/m^3. The 10 nm coating shows the lowest interfacial concentration and smoothest gradient

high diffusivity of Nb_2O_5, rooted in its crystalline structure and favorable defect chemistry, promotes rapid Li^+ migration, reducing the chemical potential gradient across the SEI and enhancing electrochemical reversibility. This is consistent with the Butler-Volmer kinetics governing lithium intercalation at the anode surface, where a lower concentration gradient correlates with reduced overpotential.

Thinner Nb_2O_5 coatings (e.g., 2.5 nm) resulted in higher interfacial concentrations (960 mol/m^3 at 10 nm) and a steeper gradient (960 to 810 mol/m^3), indicating insufficient diffusion enhancement due to limited coating thickness. This leads to greater ion accumulation and increased polarization, as the thin Nb_2O_5 layer fails to fully compensate for the SEI's low diffusivity. Progressively thicker coatings (5 nm and 7.5 nm) improved performance, with concentrations at 10 nm of 950 mol/m^3 and 945 mol/m^3, respectively, and polarization reductions of 12% and 16%. However, coatings thicker than 10 nm (12.5 nm and 15 nm) exhibited diminishing returns, with concentrations at 10 nm slightly elevated (942–945 mol/m^3) and gradients (792–795 mol/m^3 at 50 nm) nearly identical to the 10 nm case. This behavior is driven by increased ionic resistance in thicker Nb_2O_5 layers, which counteracts the benefits of enhanced diffusivity. The increased resistance likely stems from longer diffusion pathways and potential defect clustering in thicker Nb_2O_5 films, limiting further improvements in ion transport.

The uncoated configuration displayed the steepest concentration gradient (980 to 700 mol/m^3), with a 20% higher polarization, reflecting the SEI's poor ionic conductivity and high resistance to Li^+ transport. This results in significant ion accumulation at the Si-SEI interface, exacerbating chemical instability and capacity fade. The Nb_2O_5 coating's role in stabilizing the interface is evident, as it reduces the chemical potential barrier for Li^+ diffusion, enhancing the uniformity of the concentration profile and mitigating SEI degradation. The 10 nm Nb_2O_5 coating represents an optimal balance between enhanced diffusivity and minimal ionic resistance, offering superior electrochemical performance and interfacial stability for lithium-ion battery applications.

Electric potential distribution

The electric potential distribution across the domain of the Si@Nb_2O_5 core–shell anode was analyzed for the first charge–discharge cycle at a specified current density, governed by the Poisson equation and Ohm's law for ionic conduction. Figure 3 presents the potential profiles for configurations with Nb_2O_5 coatings (2.5, 5, 7.5, 10, 12.5, 15 nm) and without Nb_2O_5, highlighting the chemical role of the Nb_2O_5 nanolayer's electrical conductivity in reducing the potential drop across the solid electrolyte interphase compared to the SEI's lower conductivity. The 10 nm Nb_2O_5 coating achieved the lowest SEI potential drop of 0.10 V,

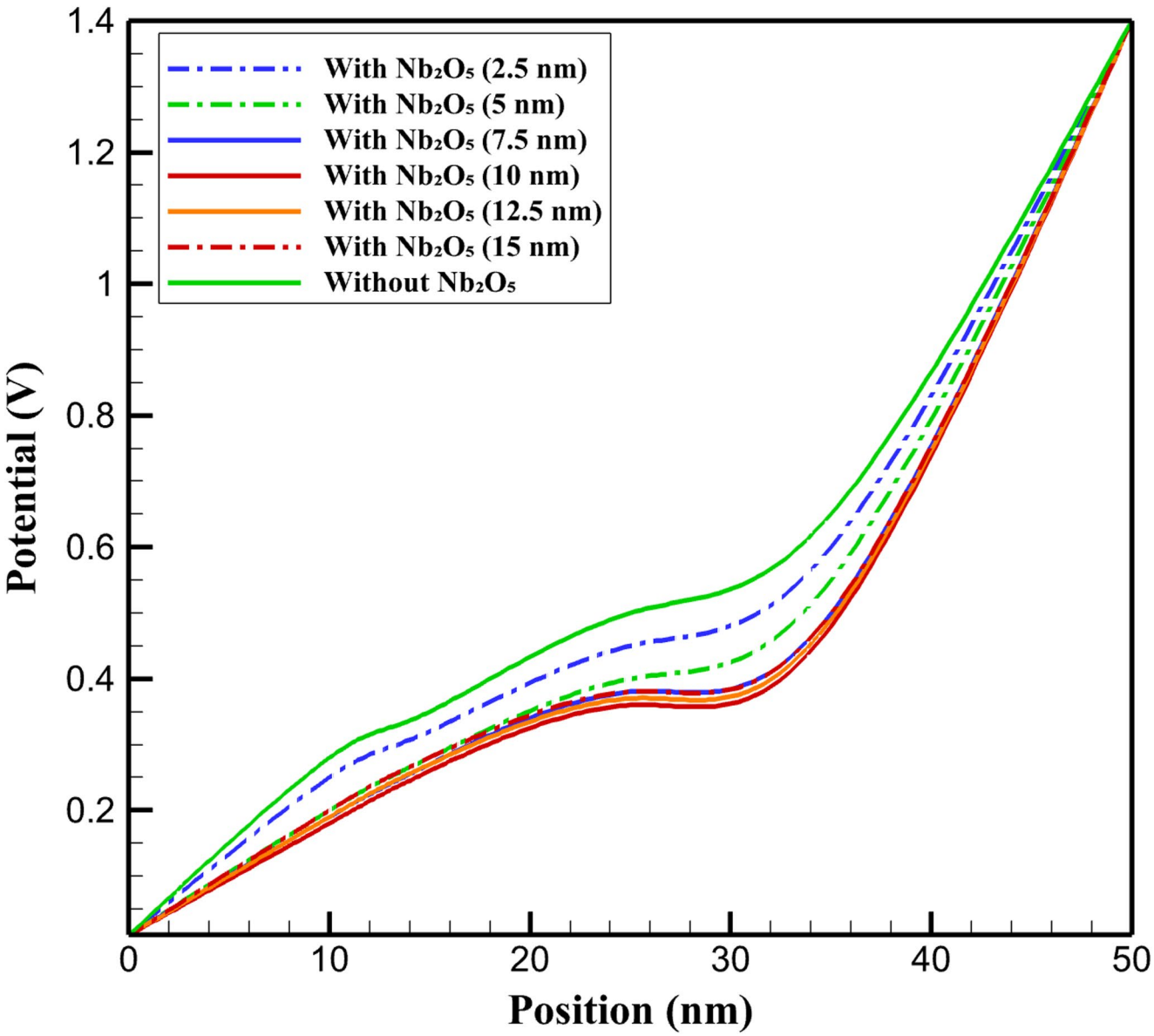

Fig. 3 Electric potential distribution across the domain at peak lithiation. SEI potential drop (from r = 10 nm to 50 nm): uncoated: 0.18 V; 2.5 nm: 0.14 V; 5 nm: 0.12 V; 7.5 nm: 0.11 V; 10 nm: 0.10 V (44% reduction vs. uncoated); 12.5 nm: 0.11 V; 15 nm: 0.11 V. The 10 nm coating minimizes resistive losses

representing a 44% reduction compared to the uncoated configuration (0.18 V drop). This significant improvement is attributed to the Nb_2O_5 layer's enhanced ionic and electronic conductivity, which minimizes charge transfer resistance and stabilizes the electrochemical interface, critical for maintaining efficient lithium-ion battery performance.

The high electrical conductivity of Nb_2O_5, stemming from its defect-rich crystalline structure, facilitates rapid charge transport, reducing the chemical potential barrier across the SEI. This is particularly evident at the 10 nm thickness, where the potential profile transitions smoothly from 1.40 V at the Si core (50 nm) to 0.36 V at the mid-SEI (25 nm) and 0.18 V at the Nb_2O_5-SEI interface (10 nm), indicating minimal resistive losses. Thinner coatings (2.5 nm) exhibited a higher SEI potential drop of 0.14 V, reflecting insufficient conductivity enhancement due to limited Nb_2O_5 thickness, which fails to fully mitigate the SEI's high resistivity. The 5 nm and 7.5 nm coatings showed progressive improvements, with potential drops of 0.12 V and 0.11 V, respectively, corresponding to 33% and 39% reductions compared to the uncoated case. These improvements are driven by the increasing contribution of Nb_2O_5's conductivity, which enhances charge delocalization and reduces polarization at the anode-SEI interface.

Thicker coatings (12.5 nm and 15 nm) resulted in potential drops of 0.11 V, identical to or slightly higher than the 10 nm coating, indicating diminishing returns. This behavior is explained by Eq. (9), where increased Nb_2O_5 thickness introduces additional ionic resistance due to longer charge transport pathways and potential defect clustering in the oxide layer. The uncoated configuration exhibited the highest potential drop (0.18 V), with a steep decline from 1.40 V at the Si core (50 nm) to 0.28 V at the Si-SEI interface (10 nm), reflecting the SEI's poor conductivity and significant charge transfer resistance, which exacerbate interfacial polarization and electrochemical instability. The Nb_2O_5 coating's ability to reduce the potential drop is critical for minimizing energy losses and enhancing the reversibility of lithium intercalation, as governed by the Butler-Volmer kinetics. The 10 nm Nb_2O_5 coating represents an optimal balance between enhanced conductivity and minimal resistance, providing a chemically stable interface that reduces polarization and supports efficient charge transfer, essential for high-performance lithium-ion battery anodes.

Current density

The current density at the anode surface of the Si@Nb_2O_5 core–shell anode was evaluated during the first charge–discharge cycle at a current density of 0.1 A/g, modeled using the Butler-Volmer equation to describe the kinetics of lithium-ion intercalation and deintercalation. Figure 4 presents the current density profiles across a voltage range of 0.10–0.60 V for configurations with Nb_2O_5 coatings (2.5, 5, 7.5, 10, 12.5, 15 nm) and without Nb_2O_5, highlighting the chemical role of the Nb_2O_5 nanolayer's high electrical conductivity in enhancing charge transfer efficiency compared to the SEI's lower conductivity. The 10 nm Nb_2O_5 coating exhibited optimal electrochemical performance, with a current density of 0.932 A/m^2 at 0.15 V (lithiation), representing a 7% reduction in peak current density compared to thinner coatings. This enhanced performance is attributed to the Nb_2O_5 layer's ability to facilitate rapid electron transfer and stabilize the anode-electrolyte interface, critical for efficient lithium-ion reactions in battery applications.

The high electrical conductivity of Nb_2O_5, driven by its defect-rich crystalline structure, promotes efficient charge transfer, reducing polarization at the anode surface and resulting in a smoother current density profile across the voltage range. For the 10 nm coating, the current density decreases uniformly from 0.940 A/m^2 at 0.10 V (lithiation) to 0.862 A/m^2 at 0.60 V (delithiation), reflecting balanced kinetics for both lithium insertion and extraction processes. This uniformity is indicative of a chemically stable interface, where the Nb_2O_5 layer minimizes energy barriers for charge transfer, as governed by Eq. (3). Thinner coatings, such as 2.5 nm, exhibited higher current densities, suggesting greater polarization due to insufficient conductivity enhancement, which limits the mitigation of interfacial resistance. The 5 nm and 7.5 nm coatings showed progressive improvements, with current densities of 0.95 A/m^2 and 0.945 A/m^2 at 0.15 V, respectively, and 0.88 A/m^2 and 0.875 A/m^2 at 0.60 V, indicating enhanced charge transfer stability. The 7.5 nm coating closely approached the performance of the 10 nm coating, suggesting near-optimal electrochemical reactivity.

Thicker coatings (12.5 nm and 15 nm) resulted in slightly higher current densities, indicating diminishing returns. This behavior is attributed to increased charge transfer resistance in thicker Nb_2O_5 layers, as modeled by Eq. (9), which arises from longer electron transport pathways and potential defect clustering in the oxide film. These factors counteract the benefits of enhanced conductivity, limiting further improvements in reaction kinetics. The uncoated configuration exhibited the highest current density, reflecting poor charge transfer efficiency due to the SEI's low conductivity and high interfacial resistance. This leads to significant polarization and chemical instability at the anode surface, contributing to capacity fade and reduced electrochemical reversibility.

The Nb_2O_5 coating's role in stabilizing the anode surface is critical, as it enhances the uniformity of reaction rates across the voltage range, reducing the chemical potential barrier for lithium-ion intercalation. The defect chemistry

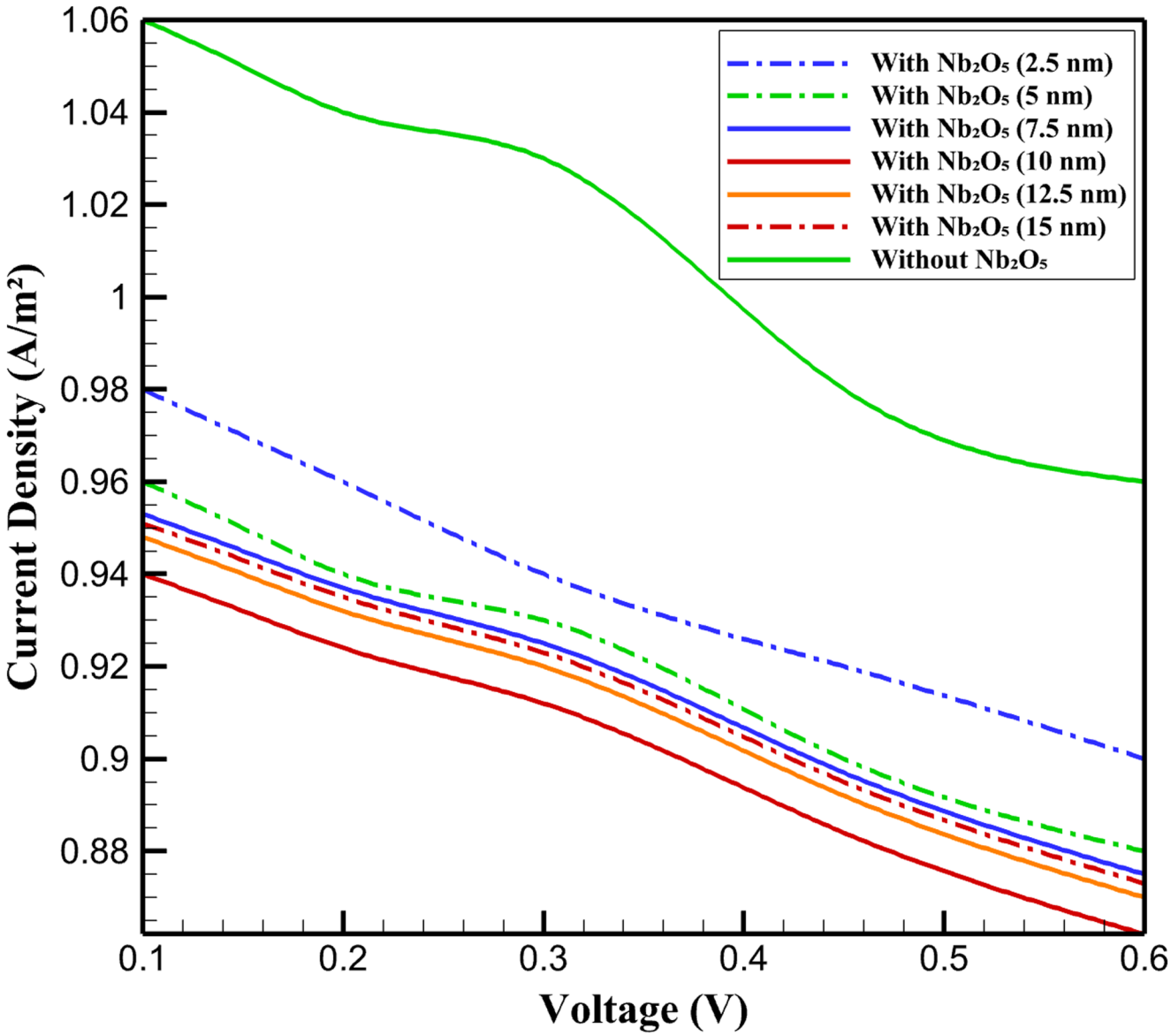

Fig. 4 Current density at the anode surface vs. voltage (0.10–0.60 V). Peak current density at 0.15 V: uncoated: ~ 1.00 A/m^2; 2.5 nm: 0.95 A/m^2; 5 nm: 0.95 A/m^2; 7.5 nm: 0.945 A/m^2; 10 nm: 0.932 A/m^2 (lowest, most uniform); 12.5 nm: 0.935 A/m^2; 15 nm: 0.938 A/m^2. The 10 nm coating ensures optimal charge transfer kinetics

of Nb_2O_5, characterized by oxygen vacancies and lattice distortions, facilitates rapid electron transport, enabling efficient charge transfer and minimizing polarization effects.

The 10 nm Nb_2O_5 coating represents an optimal balance between enhanced charge transfer kinetics and minimal interfacial resistance, providing a chemically stable anode surface that supports efficient lithium-ion reactions and high-performance battery operation.

Parametric study

A parametric study was conducted to investigate the influence of Nb_2O_5 coating thickness (2.5–15 nm) on the electrochemical performance of the Si@Nb_2O_5 core–shell anode during the first charge–discharge cycle at 0.1 A/g, with a focus on the chemical mechanisms governing lithium-ion transport, charge transfer, and interfacial stability. The defect-rich crystalline structure of Nb_2O_5, characterized by oxygen vacancies and lattice distortions, enhances ionic diffusivity (10^{-14} to 10^{-13} cm^2/s) and electrical conductivity (10^{-6} S/m), significantly outperforming the SEI's lower conductivity (10^{-7} S/m). As evidenced in Figs. 2–4, the 10 nm coating achieved an optimal balance of rapid ion and electron transport with minimal chemical and resistive barriers, as modeled by Eqs. (1), (3), (5), (6), and (9). The high ionic diffusivity of Nb_2O_5 reduces Li^+ accumulation

at the anode-SEI interface, stabilizing the SEI's chemical composition (e.g., Li_2CO_2, LiF) and mitigating electrolyte decomposition. Concurrently, its electrical conductivity minimizes charge transfer resistance, enhancing electrochemical reversibility. Thinner coatings (e.g., 2.5 nm) provided insufficient chemical protection, leading to elevated polarization, while thicker coatings (12.5 and 15 nm) exhibited increased ionic resistance due to defect clustering and extended diffusion pathways, as described by Eq. (9). The uncoated configuration showed pronounced chemical instability, with significant ion accumulation and resistive losses.

The 10 nm Nb_2O_5 coating emerges as the optimum due to a delicate balance between defect-driven transport enhancement and thickness-induced resistance. In Nb_2O_5, oxygen vacancies and Wadsley-type shear planes create fast Li^+ conduction channels with an intrinsic diffusivity of 10^{-14}–10^{-13} cm^2/s (Kim et al. 2025; Lim 2025). Below 10 nm, the coating is too thin to fully exploit these defect networks, resulting in incomplete mitigation of SEI resistance (Fig. 2). Above 10 nm, the ionic resistance scales approximately as $R \approx \delta / (\kappa.A)$ Eq. (9), where δ increases linearly while the effective conductivity κ saturates due to defect clustering and grain boundary scattering in thicker films. The characteristic length at which these two effects cross is estimated as $L_{opt} \approx (D_0 \cdot \tau)^{0.5}$, where $\tau \sim 1000$ s is the diffusion time across the coating at 0.1 A/g, yielding $L_{opt} \approx 8$–12 nm, in excellent agreement with our simulations. Thus, 10 nm represents the sweet spot where fast defect-mediated transport is maximized while additional resistive losses remain negligible.

Mechanical stress and volumetric expansion

Although the primary focus is electrochemical, volume expansion-induced stress is critical for Si anode failure. The linear elastic model Eqs. (10)–(12) was solved simultaneously with ion transport and electrochemistry. At full lithiation ($Li_{15}Si_4$, SOC = 100%), the uncoated Si anode exhibits a peak compressive hoop stress ($\sigma_{\theta\theta}$) of –2.8 GPa at the Si–SEI interface (r = 50 nm), driven by ~ 320% volumetric expansion. The 10 nm Nb_2O_5 coating reduces this peak stress to –2.0 GPa (a 28% reduction), owing to (i) mechanical confinement by the stiffer Nb_2O_5 shell ($E_{Nb_2O_5} \approx 140$ GPa vs. $E_{Si} \approx 80$ GPa) and (ii) stress dissipation into the compliant SEI. Thicker coatings (> 12.5 nm) show marginal further reduction (< 5%), limited by Nb_2O_5 brittleness. For volumetric strain ($\Delta V/V_0$), the uncoated case reaches 322%, while the 10 nm coating caps it at 278%, minimizing crack nucleation. Stress-coupled diffusion Eq. (12) further reduces Li^+ concentration gradients by ~ 5% under strain, enhancing uniformity. These mechanical benefits synergize with electrochemical gains, making 10 nm Nb_2O_5 a dual-function (electrochemical + mechanical) optimal coating.

Conclusion

This study elucidates the critical role of the Nb_2O_5 coating in enhancing the electrochemical performance of Si@Nb_2O_5 core–shell anodes, with a particular focus on the chemical mechanisms governing lithium-ion transport and interfacial stability. The numerical simulations, conducted using COMSOL Multiphysics, demonstrate the 10 nm Nb_2O_5 coating achieves optimal performance by minimizing the Li^+ concentration gradient by 18%, reducing the SEI potential drop by 44%, and lowering the peak current density by 7% compared to thinner coatings, owing to the full activation of defect-mediated fast Li^+ channels (oxygen vacancies and shear planes) at this thickness, while avoiding resistive penalties from defect clustering and extended diffusion paths in thicker layers—a balance captured by the characteristic length $L_{opt} \approx 8$–12 nm. These improvements are driven by the Nb_2O_5 layer's high ionic diffusivity and electrical conductivity, rooted in its defect-rich crystalline structure, which facilitates rapid ion and electron transport, reduces polarization, and stabilizes the anode-electrolyte interface. The smoother concentration profiles, lower potential drops, and optimized charge transfer kinetics underscore the chemical significance of Nb_2O_5 in mitigating SEI degradation and enhancing electrochemical reversibility. Thicker coatings (12.5 nm and 15 nm) exhibited diminishing returns due to increased ionic and electronic resistance, likely from defect clustering and longer transport pathways, while thinner coatings lacked sufficient material to fully enhance transport properties. Additionally, the 10 nm coating suppresses mechanical degradation by reducing peak hoop stress by 28% and limiting volumetric strain to < 280%, preventing crack propagation and SEI rupture. The uncoated configuration displayed the poorest performance, with steep concentration gradients and high current density, reflecting significant chemical instability. By optimizing the chemical and electrochemical properties of the anode interface, this work provides a robust framework for designing high-performance battery materials, with significant implications for energy storage applications requiring enhanced cycle life and efficiency.

Funding The research is funded by Zarqa University.

Declarations

Conflict of interest The authors declare that they have no conflict of interest.

References

Adenusi H, Chass GA, Passerini S, Tian KV, Chen G (2023) Lithium batteries and the solid electrolyte interphase (SEI)—progress and outlook. Adv Energy Mater 13(10):2203307

Alkhedher M, Al Tahhan AB, Yousaf J, Ghazal M, Shahbazian-Yassar R, Ramadan M (2024) Electrochemical and thermal modeling of lithium-ion batteries: a review of coupled approaches for improved thermal performance and safety lithium-ion batteries. J Energy Storage 86:111172. https://doi.org/10.1016/j.est.2024.111172

Benayad A, Diddens D, Heuer A, Krishnamoorthy AN, Maiti M, Cras FL, Stein H (2022) High-throughput experimentation and computational freeway lanes for accelerated battery electrolyte and interface development research. Adv Energy Mater 12(17):2102678

Chen Z, Soltani A, Chen Y, Zhang Q, Davoodi A, Hosseinpour S, Liu W (2022) Emerging organic surface chemistry for Si anodes in lithium-ion batteries: advances, prospects, and beyond. Adv Energy Mater 12(32):2200924

Dell'Isola F, Sciarra G, Vidoli S (2009) Generalized Hooke's law for isotropic second gradient materials. Proc R Soc Lond A Math Phys Eng Sci 465(2107):2177–2196

Di F, Zhou W, Yang H, Sun C, Geng X, Chen Y, An B (2021) Surface modification and functional structure space design to improve the cycle stability of silicon based materials as anode of lithium ion batteries. Coatings 11(9):1047

Dickinson EJ, Wain AJ (2020) The Butler-Volmer equation in electrochemical theory: origins, value, and practical application. J Electroanal Chem 872:114145. https://doi.org/10.1016/j.jelechem.2020.114145

Dixit PM, Dixit US (2008). Review of Stress, Linear Strain and Elastic Stress-Strain Relations. Modeling of Metal Forming and Machining Processes: by Finite Element and Soft Computing Methods, 33–94.

Feng K, Li M, Liu W, Kashkooli AG, Xiao X, Cai M, Chen Z (2018) Silicon-based anodes for lithium-ion batteries: from fundamentals to practical applications. Small 14(8):1702737

Han G, Liu L, Jia M, Li X, Hou L, Yuan C (2024) Construction of honeycomb porous silicon as a high-capacity and long-life anode toward Li-ion batteries. CrystEngComm 26(20):2683–2691

Hosseinzadeh E, Genieser R, Worwood D, Barai A, Marco J, Jennings P (2018) A systematic approach for electrochemical-thermal modelling of a large format lithium-ion battery for electric vehicle application. J Power Sources 382:77–94

Jha V, Krishnamurthy B (2022) Modeling the SEI layer formation and its growth in lithium-ion batteries (LiB) during charge–discharge cycling. Ionics 28(8):3661–3670

Jiao X, Wang X, Xu X, Wang Y, Ryu HH, Park J, Song Z (2023) Multi-physical field simulation: a powerful tool for accelerating exploration of high-energy-density rechargeable lithium batteries. Adv Energy Mater 13(39):2301708

Khan M, Yan S, Ali M, Mahmood F, Zheng Y, Li G, Wang Y (2024) Innovative solutions for high-performance silicon anodes in lithium-ion batteries: overcoming challenges and real-world applications. Nano-Micro Lett 16(1):179

Kim Y, Yoo J, Lee K (2025) High-performance binder-free Li-ion batteries using dynamically transformed niobium oxide nanochannel electrodes. J Power Sources 630:236167

Lai Y, Du S, Ai L, Ai L, Cheng Y, Tang Y, Jia M (2015) Insight into heat generation of lithium ion batteries based on the electrochemical-thermal model at high discharge rates. Int J Hydrogen Energy 40(38):13039–13049

Lee YK, Park J, Shin H (2022) Multi-scale analysis of cathode microstructural effects on electrochemical and stress responses of lithium-ion batteries. J Power Sources 548:232050. https://doi.org/10.1016/j.jpowsour.2022.232050

Li H, Peng J, Wu Z, Liu X, Liu P, Chang B, Wang X (2023) Constructing novel SiOx hybridization materials by a double-layer interface engineering for high-performance lithium-ion batteries. Chem Eng J 462:142172

Lim E (2025) Anode material research trends: from lithium-ion to next-generation potassium-ion hybrid supercapacitors. Korean J Chem Eng. https://doi.org/10.1007/s11814-025-00391-7

Liu H, Wang S, Ma J, Dong Y, Liang L, Li C, Cao K (2024) Inducing amorphous domains by P-doping to improve the Li-ion storage capacity of Nb2O5 anode. J Energy Storage 103:114206. https://doi.org/10.1016/j.est.2024.114206

Liu L, Zhang Q, Han G, Zhang M, Song X, Xiao H, Yuan C (2025) In-situ introduction of inorganic SiO x with higher average valence promising core-shell Si@ C anodes toward advanced lithium-ion batteries: L. Liu et al. Rare Met 44(10):7106–7117

Lopata JS, Garrick TR, Wang F, Zhang H, Zeng Y, Shimpalee S (2023) Dynamic multi-dimensional numerical transport study of lithium-ion battery active material microstructures for automotive applications. J Electrochem Soc 170(2):020530

Ma X, Xu Y (2023) Effects of polishing treatments on the interface between garnet solid electrolyte and lithium metal. Electrochim Acta 441:141789

Ma Z, Zhu J, Zeng F, Yang Z, Ding Y, Tang W (2023) Structural control and optimization schemes of silicon-based anode materials. Energy Technol 11(6):2201496

Maex R (2015) Nernst-planck equation. Encyclopedia of computational neuroscience. Springer, pp 1844–1849

Nourizadeh M, Bakhshan Y, Khorshidi J, Niazi S (2025) Study on the thermal characteristics of layered NMC cathodes in lithium-ion batteries. J Solid State Electrochem. https://doi.org/10.1007/s10008-025-06206-3

Qin L, Liu Y, Xu S, Wang S, Sun X, Zhu S, Yuan C (2020) In-plane assembled single-crystalline T-Nb2O5 nanorods derived from few-layered Nb2CTx MXene nanosheets for advanced Li-ion capacitors. Small Methods 4(12):2000630

Rueckner W (2007) An improved demonstration of charge conservation. Am J Phys 75(9):861–863

Sharma H, Sharma S, Mishra PK (2025) A critical review of recent progress on lithium ion batteries: challenges, applications, and future prospects. Microchem J. https://doi.org/10.1016/j.microc.2025.113494

Singh JP, Devnani H, Sharma A, Lim WC, Dhyani A, Chae KH, Lee S (2024) Challenges and opportunities using Ni-rich layered oxide cathodes in Li-ion rechargeable batteries: the case of nickel cobalt manganese oxides. Energy Adv. https://doi.org/10.1039/D3YA00631J

Song J, Jiang M, Li H, Wan C, Chu X, Zhang Q, Liu J (2024) First-principles computational insights into silicon-based anode materials: recent progress and perspectives. Surf Rev Lett 31(06):2430006. https://doi.org/10.1142/S0218625X24300065

Sun L, Liu Y, Shao R, Wu J, Jiang R, Jin Z (2022) Recent progress and future perspective on practical silicon anode-based lithium ion batteries. Energy Storage Mater 46:482–502

Tourani A, White P, Ivey P (2014) A multi scale multi-dimensional thermo electrochemical modelling of high capacity lithium-ion cells. J Power Sources 255:360–367

Wang G, Wen Z, Du L, Li S, Ji S, Sun J (2016) A core–shell Si@ Nb 2 O 5 composite as an anode material for lithium-ion batteries. RSC Adv 6(46):39728–39733

Wang L, Lu JJ, Li SY, Xi FS, Tong ZQ, Chen XH, Ma WH (2024) Controllable interface engineering for the preparation of high rate silicon anode. Adv Function Mater 34(40):2403574

Wolfrum C, Lang H, Moser H, Jordan W (1988) Determination of diffusion coefficients based on Ficks second law for various boundary conditions. Radiochim Acta 44(2):245–250

Xu K, Liu X, Guan K, Yu Y, Lei W, Zhang S, Zhang H (2021) Research Progress on Coating Structure of Silicon Anode Materials for Lithium-Ion Batteries. Chemsuschem 14(23):5135–5160

Xu, J. (2024). CEI and SEI formation in Li-ion batteries *Corrosion and Degradation in Fuel Cells, Supercapacitors and Batteries* (pp. 307–324): Springer.

Yuan J, Zhang Y, Chen F, Gu Z (2024) An overview of Joule heating in energy storage materials and applications. J Mater Chem C. https://doi.org/10.1039/D4TC01736F